JACS
JOURNAL OF THE AMERICAN CHEMICAL SOCIETY
Article
pubs.acs.org/JACS

RNA Encapsidation by SV40-Derived Nanoparticles Follows a Rapid Two-State Mechanism

Stanislav Kler,[†,▽] Roi Asor,[‡,▽] Chenglei Li,[§] Avi Ginsburg,[‡,∥] Daniel Harries,[‡,⊥] Ariella Oppenheim,*[,†] Adam Zlotnick,*[,§,#] and Uri Raviv*[,‡]

[†]Department of Hematology, Hebrew University—Hadassah Medical School, Jerusalem, Israel 91120
[‡]Institute of Chemistry, The Hebrew University of Jerusalem, Israel 91904
[§]Department of Molecular and Cellular Biochemistry, Indiana University, Bloomington, Indiana 47405, United States
[∥]The School of Drug Research, The Hebrew University of Jerusalem, Israel 91904
[⊥]The Fritz Haber Research Center, The Hebrew University of Jerusalem, Israel 91904
[#]Department of Biology, Indiana University, Bloomington, Indiana 47405, United States

Supporting Information

ABSTRACT: Remarkably, uniform virus-like particles self-assemble in a process that appears to follow a rapid kinetic mechanism. The mechanisms by which spherical viruses assemble from hundreds of capsid proteins around nucleic acid, however, are yet unresolved. Using time-resolved small-angle X-ray scattering (TR-SAXS), we have been able to directly visualize SV40 VP1 pentamers encapsidating short RNA molecules (500mers). This assembly process yields $T = 1$ icosahedral particles comprised of 12 pentamers and one RNA molecule. The reaction is nearly one-third complete within 35 ms, following a two-state kinetic process with no detectable intermediates. Theoretical analysis of kinetics, using a master equation, shows that the assembly process nucleates at the RNA and continues by a cascade of elongation reactions in which one VP1 pentamer is added at a time, with a rate of approximately 10^9 M^{-1} s^{-1}. The reaction is highly robust and faster than the predicted diffusion limit. The emerging molecular mechanism, which appears to be general to viruses that assemble around nucleic acids, implicates long-ranged electrostatic interactions. The model proposes that the growing nucleoprotein complex acts as an electrostatic antenna that attracts other capsid subunits for the encapsidation process.

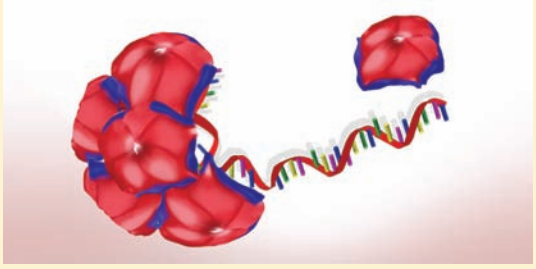

INTRODUCTION

Viruses are evolved examples of self-assembled structures that are remarkably sophisticated biological machines. This ability to self-assemble can be harnessed for nano- and biotechnology. Indeed, viral capsids and capsid proteins have been used to assemble structures for guided synthesis of inorganic and organic nanostructures,[1,2] as cages for packaging cargos,[3,4] and as vectors for gene therapy.[5−7] The mechanism of packaging even biologically relevant nucleic acids, however, remained unknown.

An attractive candidate for nanostructural manipulation is the SV40 virus, a small nonenveloped virus belonging to the polyomavirus family. SV40 has a circular double-stranded (ds) DNA genome of 5,243 base pairs compacted by histone octamers to a nucleosomal structure similar to cellular chromatin.[8,9] The 48 nm diameter viral capsid, surrounding the viral minichromosome, is composed of three proteins, VP1, VP2, and VP3. VP1 forms the outer shell while VP2 and VP3 are located internally to VP1 and help bridge it to the chromatin core. Nonetheless, VP1 alone binds DNA with high affinity.[10] VP1 monomers are tightly bound in pentamers ($VP1_5$) through interdigitating β-strands[11] formed immediately following translation.[12] On the basis of this architecture, SV40 capsids are composed of 72 VP1 pentamers arranged in a $T = 7$ lattice.[11,13]

Recombinant $VP1_5$ also assembles cooperatively around circular ds-DNA, to form an icosahedral structure that is similar to wild-type (wt) SV40.[14,15] Such virus-like particles (VLPs) may be used as vectors for gene delivery[5,6] as well as an experimental model system to study assembly reactions.[15] We recently demonstrated a requirement of a nucleic acid for uncatalyzed assembly of purified VP1 under physiological conditions (150 mM NaCl at pH 7.2). We proposed that the nucleic acid served as a nucleation center and/or a scaffold for assembly.

The specific mechanism(s) of how viruses assemble on nucleic acids remains an open question. Experience with assembly of empty capsids[16] suggests that assembly is nucleated and based on weak interactions of multivalent subunits. Weak association allows error correction of misincorporated subunits.[17,18] Nucleation prevents a situation where there may be many partial capsids but no complete ones. Nucleation and weak association result in assembly reactions that appear two-state, with few if any intermediates transiently detectable.[19−21]

Received: November 25, 2011
Published: February 13, 2012

   dx.doi.org/10.1021/ja2110703 | J. Am. Chem. Soc. 2012, 134, 8823−8830

Many self-assembling virus capsid proteins, including SV40 $VP1_5$, have nucleic acid binding domains that will certainly affect the details of assembly. Observations of assembly reactions that have been given time to equilibrate suggest complex, cooperative behavior. For example, RNA titrations by hepatitis B virus capsid protein appear two-state,[22] whereas titrations with cowpea chlorotic mottle virus capsid protein (which has much weaker self-association[23]) appear to be gradual.[24] Describing the pathway of assembly and encapsidation, however, requires rigorous kinetic analysis.

Here we report self-assembly of $T = 1$ VLPs from SV40 $VP1_5$, induced by a short single-stranded (ss) RNA polymer. The short ssRNA substrate allowed us to examine the simplest case reaction of dodecahedral assembly, where all pentamers are equivalent. Conversely, assembly with dsDNA is much more complicated: dsDNA leads to a 72 pentamer complex with several different classes of pentamer−pentamer interactions. An additional issue is the work required to bend the dsDNA (with a persistence length of about 50 nm) to fit into an SV40 capsid, with an inner diameter of about 40 nm. To ensure that we could describe progression of the reaction and the presence or absence of intermediates, we followed assembly using high-resolution synchrotron time-resolved small-angle X-ray scattering (TR-SAXS). On the basis of fitting TR-SAXS data to a master equation model of capsid assembly, VLP formation appeared to be nucleated, where the nucleation step was differentiated from elongation on the basis of kinetics. Assembly rate constants were very fast, leading us to suggest that long-range (electrostatic) interactions play a critical role in assembly. The strong negative surface charge, common to most virus capsids, may thus contribute to attracting reactants that facilitate formation of viruses and VLPs, *in vivo* and *in vitro*.

MATERIALS AND METHODS

Protein and RNA for Assembly Reactions. SV40 VP1 VLPs were produced in *Spodoptera frugiperda* 9 (Sf9) insect cells and produced as previously described.[15] Pentamers were obtained by dissociating VLPs by dialysis first against 20 mM Tris-Cl, pH 8.9, 50 mM NaCl, 2 mM DTT (dissociation buffer) with 5 mM EDTA and then against dissociation buffer with 2 mM EDTA at 4 °C. The dialysate was centrifuged at 20,000 g for 30 min at 4 °C to sediment aggregated protein. Clarified supernatant was quantified by UV absorbance, using an extinction coefficient of ε_{280} = 32,890 M^{-1} cm^{-1} per VP1 monomer.[25]

We used yeast 75 nucleotides tRNA, 524 nucleotide RNA (500mer), and 814 nucleotides RNA (800mer) as templates for SV40 VP1 assembly. Yeast 75 nt tRNA was purchased from Ambion. 500mer and 800mer RNAs were *in vitro* transcribed from linearized pETc11-Cp149 using a MegaScript T7 kit (Ambion). Though not fully tested, it is likely that the actual sequence does not make a significant contribution to the details of assembly.

Equilibrated Assembly Reactions. Disassembled VP1 pentamers were mixed with RNA in 2 × assembly buffer (250 mM NaCl, 100 mM MOPS pH 7.2). Samples were examined by electrophoretic mobility shift assay (EMSA), transmission electron microscopy (TEM), and size exclusion chromatography with absorbance or multiangle laser light scattering detectors (SEC or SEC-MALLS). For EMSA, samples were electrophoresed through 0.6% agarose gel using a TAE buffer system for 1 h at 100 V constant voltage followed by ethidium bromide staining.[24] Samples for TEM were adsorbed to freshly glow discharged, Formvar-carbon coated copper grids (EM sciences) for 3 min and stained with 2% uranyl acetate for 30 s and washed with deionized water. Samples were air-dried and visualized on JEOL JEM1010.

Size exclusion chromatography was performed using Bio SEC-5 columns (7 and 14 mL) with a 500 Å pore size (Agilent Technologies) equilibrated with assembly buffer. For absorbance analysis we used a Shimadzu HPLC with a diode array detector. For SEC-MALLS we used a Shimadzu HPLC pump with DAWN HELEOS II light scattering and Optilab Rex refractive index detectors in series (both from Wyatt).

Data Collection for SAXS. SAXS measurements were performed at beamline ID02 in ESRF (Grenoble, France) with 10 keV X-rays from a $Si_{1,1,1}$ monochromator. Silver behenate was used as a standard to determine the sample to detector distance. Data were recorded with a Fast-Readout, Low-Noise (FReLoN) Kodak KAF-4320 CCD-based sensor.[26−28]

To determine the steady-state scattering of $VP1_5$ solution and RNA-containing capsids, we used a flow-through setup, composed of a 1.2 mm inner diameter quartz capillary connected to a syringe. RNA-containing capsids were assembled by mixing equal volumes of 10 μM VP1 pentamers with 0.6 μM RNA in assembly buffer. After an incubation of 20 min, the solution was injected into the flow-through setup and SAXS scans were recorded. The scattering signal from an excess of 1.4 μM $VP1_5$ was subtracted to obtain the signal of the pure capsid. At equilibrium, most if not all the RNA was consumed; hence, the contribution from unassembled RNA chains to the signal was negligible.

TR-SAXS measurements were recorded by mixing 100 μL of 15 μM $VP1_5$ and 100 μL of 1 μM 500mer RNA, using a BioLogic SFM-400 stopped-flow instrument and a 1.6 mm quartz capillary. Several regimes of data collection were followed to produce the final data set. For four sets of reactions, SAXS was measured for 5 ms starting after delays of 35, 85, 135, or 185 ms and then at intervals of 200 ms, thereby covering the first 2 s of assembly at a sampling density of 50 ms. The fifth set of reactions was measured for 5 ms starting after a delay of 30 ms followed by 0.995 s intervals, for a total of 1 min.

The 2D scattering patterns were radially integrated.[29] The scattering intensity, I, was plotted as a function of the magnitude of the momentum transfer vector, q, and analyzed using the X+ software.[26,30] A form-factor model of multiple concentric spherical shells with smoothly varying electron density profiles, represented by hyperbolic tangents (eq 1), was fit to the steady-state VLP data, as described[26,30]

$$\Delta\rho(r) = 0.5\{\Delta\rho_1 + \sum_{i=1}^{N-1} (\Delta\rho_{i+1} - \Delta\rho_i) \tanh[s_i(r - R_i)]\} \quad (1)$$

$\Delta\rho(r)$ indicates the radial electron density contrast with respect to the solvent (buffer). The index i represents the i-th layer in the sphere, with an outer radius, R_i, an electron density contrast, $\Delta\rho_i$, and connection to the subsequent layer $(i + 1)$ by a slope s_i. $\Delta\rho_N = 0$ and corresponds to the solvent electron density contrast. The form-factors of the smooth $\Delta\rho(r)$ functions were calculated by discretizing the profiles and transforming them to a sum of Heaviside Step functions that can be analytically solved.[26,30]

RESULTS

Assembly on Short RNA. *In vitro* assembly of SV40 VP1 pentamers ($VP1_5$) on nucleic acid is controlled by protein−protein interactions and the nature of the nucleic acid scaffold.[25] Short, flexible RNA molecules were expected to favor local interactions, as they would be too small to interact with the complement of 72 pentamers of the wt SV40 capsid. Binding of VP1 to short RNA was evaluated by electrophoretic mobility shift assay (EMSA), titrating a constant concentration of nucleic acid with increasing amounts of $VP1_5$. Titrations (Figure 1A and Supporting Information Figure S1A) showed a bimodal distribution of free and VP1-bound short RNA for three different RNA substrates, tRNA, and longer 524 nucleotide and 814 nucleotide substrates. The decrease in the amount of free RNA, measured by ethidium bromide (EtBr) fluorescence in gels, was proportional to the amount of added $VP1_5$, though some smearing was also evident. For all three RNAs, at high $VP1_5$ concentrations, the majority of the EtBr staining material ran as a single slow migrating band.

dx.doi.org/10.1021/ja2110703 | J. Am. Chem. Soc. 2012, 134, 8823−8830

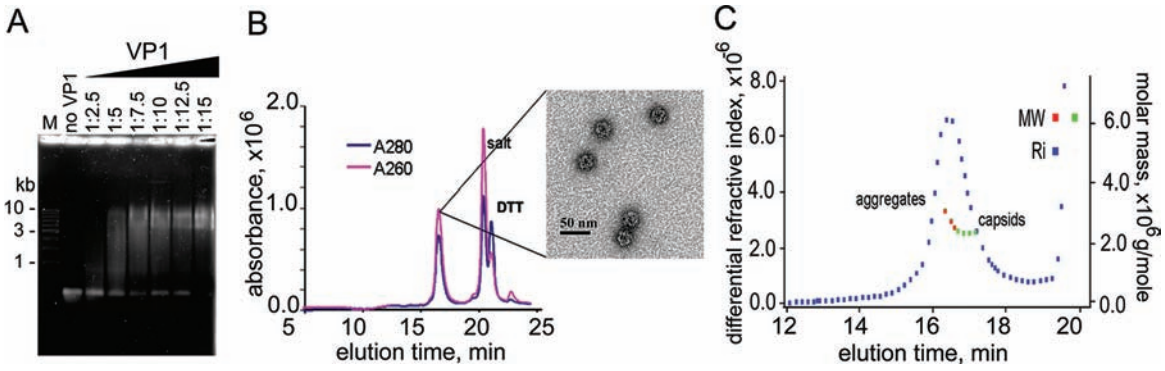

Figure 1. Assembly of $VP1_5$ with 524 nt RNA molecules, stoichiometry, and mass of 22 nm capsids. (A) Titration of 524 nt RNAs with VP1 pentamers. Electrophoretic mobility shift assay (EMSA) was analyzed by 0.6% agarose gels. (B) Size exclusion chromatography (SEC) of capsids assembled on 524 nt RNA. The A260/A280 absorbance ratio corresponds to 12 VP1 pentamers per one RNA molecule. Inset: TEM image of the fraction collected from the absorbance peak, showing only 22 nm capsids. (C) Multiangle laser light scattering (MALLS) of the capsids assembled on 524 nt RNA. The molecular weight of the capsids is 2.6 MDa, as expected for $T = 1$ capsid.

Size and Structure of the Capsids. Transmission electron microscopy (TEM) showed that assembly on all three short RNA substrates resulted in capsids of ca. 22 nm (Figure 1B and Supporting Information Figures S1B and S2), consistent with $T = 1$ particles. The 22 nm particles were first characterized by size exclusion chromatography (SEC) using an HPLC equipped with a diode array absorbance detector to determine the ratio of $VP1_5$ to nucleic acid in the capsids fraction[22] (Figure 1B and Supporting Information Figure S2). After correction for light scattering, the 260/280 absorbance ratio for the particles assembled on the 524 nt RNA was 1.357 ± 0.001, corresponding to one RNA molecule for every 11.5 pentamers, close to the 12 pentamers required for a $T = 1$ capsid (the expected 260/280 absorbance ratio for a $T = 1$ particle is 1.33). The 260/280 absorbance ratio for the particles assembled on 75 nt RNA was 1.19 (Supporting Information Figure S2), corresponding to two RNA molecules per capsid. To further characterize the 22 nm particles, we focused further experiments on reactions with the 524 nt RNA (hereafter 500mer RNA). The reaction products appeared to be homogeneous by both TEM and SAXS (described later).

In additional experiments, SEC with multiangle laser light scattering (SEC-MALLS) was used to measure the weight-average molecular weight (M_W) and diameter of solute in the capsid fractions. The beginning of the capsid peak included some high molecular weight aggregates and was excluded from the M_W calculation. For fractions eluted from 16.7 to 17.3 min (Figure 1C), the M_W and diameter were homogeneous. On the basis of the angular dependence of scattering, the capsid diameter was 22.4 ± 0.4 nm. The weight-average molecular weight was 2.6 ± 0.03 MDa (Figure 1C). This molecular weight is very close to the calculated weight of one 500mer RNA molecule and twelve 210 kDa VP1 pentamers (150 kDa + 12 × 210 kDa = 2.67 MDa). These results are consistent with assignment of the 22 nm particles as $T = 1$ icosahedra.

SAXS of Pentamers and $T = 1$ Capsids. To describe the X-ray scattering solute to a first approximation, a form-factor of multiple concentric spherical shells with smoothly varying electron density profiles was fit to the data, as previously described.[26]

SAXS of the 500mer RNA–$VP1_5$ complex (Figure 2) correlates with VLPs that have an outer diameter of 24.5 nm, consistent with TEM and MALLS (Figure 1 and Supporting Information Figure S1). At low q values, the scattering intensity is well fit by a multishell spherical model with high electron density at the center,

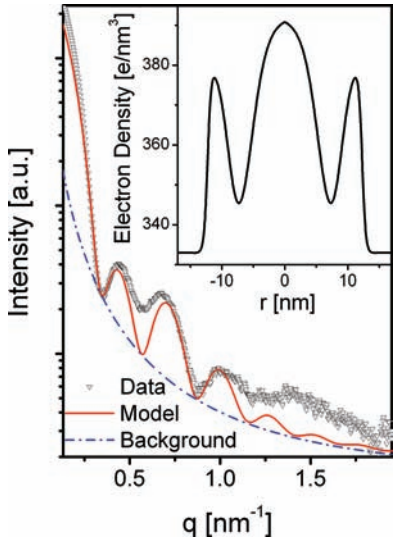

Figure 2. Radially integrated solution small X-ray scattering (SAXS) intensity from steady-state ($T = 1$) 500mer RNA VLPs (open symbols). The solid curve is the best fitted form-factor model of multiple spherical shells with smoothly varying radial electron density profiles, represented by hyperbolic tangent functions (eq 1) and shown in the inset. The broken curve shows the assumed power-law background given by $0.261q^{-2.061}$ + 0.142. The best fitted parameters for eq 1 are the following: $\Delta\rho_1 = 58.9$ e/nm^3, $\Delta\rho_2 = -18.0$ e/nm^3, $\Delta\rho_3 = 48.5$ e/nm^3 (the electron density of the buffer is assumed to be similar to that of water: 333 e/nm^3): $R_1 = 5.7$ nm, $R_2 = 8.7$ nm, $R_3 = 12.2$ nm, $s_1 = 0.4$, $s_2 = 0.5$, and $s_3 = 1.7$.

enveloped by a lower density layer, and followed by a high electron density outer layer. This would correspond to a protein shell surrounding an RNA core. The particles appear to be monodisperse, as indicated by the adequate fit of the data at the first and third minima. At high resolution (high q values), the simple spherical multishell model is insufficient to well fit the data.

TR-SAXS of Assembly. TR-SAXS of the reaction of $VP1_5$ and 500mer, observed over a period of 1 min, using a stopped-flow setup, shows a progressive change in the angular dependence of scattering. Overlays of a series of time-resolved measurements (Figure 3A) of the reaction show an isosbestic point at $q \approx 0.25$ nm^{-1}. Isosbestic points suggest that two states dominate the reaction. Intermediate structures are likely to form but remain at low concentrations and, hence, negligibly contribute to the scattering signal.

dx.doi.org/10.1021/ja2110703 | J. Am. Chem. Soc. 2012, 134, 8823–8830

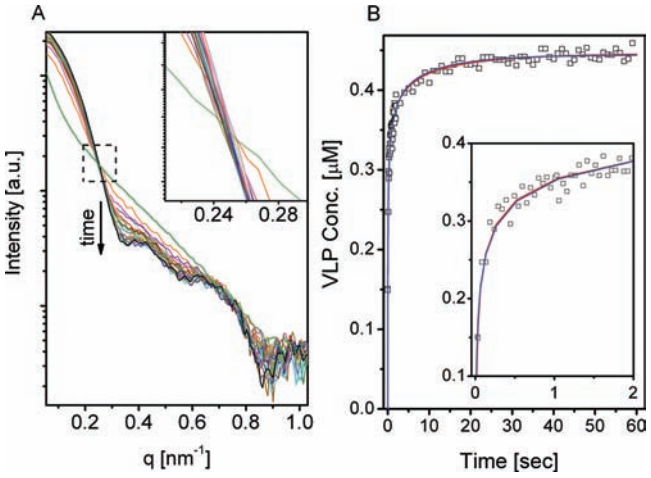

Figure 3. TR-SAXS data and kinetic analysis. (A) Radially integrated TR-SAXS measurements during the assembly process of the $T = 1$ VLPs. The time, t, elapsed after mixing 0.5 μM 500mer RNA and 7.5 μM VP1 pentamers is between 35 ms (orange curve) and 59 s (black curve). The signal that corresponds to $t = 0$ (green curve) is represented by the sum of the measured scattering intensities of a solution of 7.5 μM VP1 pentamers and a solution of 0.5 μM 524 nt ssRNA. The inset shows the isosbestic point at $q \sim 0.25$ nm^{-1} on an expanded scale. For clarity, the figure shows only selected time points. (B) Concentration of the formed $T = 1$ RNA VLPs as a function of time, t, fit to predicted assembly kinetics (eqs 6 and 7). The inset shows the first 2 s on an expanded scale. The concentrations were obtained by fitting the scattering curves shown in part A to eq 3 (Supporting Information Figure S4). The reaction kinetics were modeled assuming the RNA initially nucleated either with a VP1 pentamer (blue curve), a dimer of pentamers (red curve), or a trimer of pentamers (black solid curve; not seen due to overlap with the red curve). Separate curve fits, residuals, and the negligible fraction of intermediate structures in each model are shown in Supporting Information Figure S6.

For a two-state reaction, TR-SAXS intensities can be modeled as a sum of the intensities of the reactant and product as follows:

$$I(q, t) = \alpha(t)I_{\mathrm{VLP}}(q) + \beta(t)I_{\mathrm{pentamers}}(q) + \gamma(t)I_{\mathrm{RNA}}(q) \quad (2)$$

In eq 2, $I_{\mathrm{VLP}}(q)$, $I_{\mathrm{pentamers}}(q)$, and $I_{\mathrm{RNA}}(q)$ are normalized basis spectra for capsid, $VP1_5$, and RNA, respectively (Figure 2 and Supporting Information Figure S3). The time-dependent coefficients α, β, and γ represent the time-dependent concentrations. As we have observed that VLPs are comprised of one RNA molecule and 12 $VP1_5$, the progression of scattering should be well-described by a single free parameter:

$$I(q, t) = \alpha(t)I_{\mathrm{VLP}}(q) + [\beta_0 - 12\alpha(t)]I_{\mathrm{pentamers}}(q) + [\gamma_0 - \alpha(t)]I_{\mathrm{RNA}}(q) \quad (3)$$

where β_0 and γ_0 are the initial concentrations of the VP1 pentamers and RNA, respectively (there were no VLPs at time zero).

Indeed, the fit of the normalized basis spectra of pure reaction components (Supporting Information Figure S3) to the scattering data of Figure 3A are consistent with a two-state reaction as describe by eq 3 (Supporting Information Figure S4). Furthermore, the observed isosbestic point is unlikely to form with more than two dominating states (reactants and product, as in eq 3).

From fitting the data to eq 3, we obtained the concentration of RNA-filled VLPs as a function of time (Figure 3B). Individual experiments were very consistent; the reaction time course represents data from five individual assembly reactions with measurements taken at different delays. At 30 ms, there is more than 0.15 μM capsid out of a theoretical maximum of 0.5 μM. The first 2−3 s of the reaction produces nearly 90% of the steady state VLP concentration. The concentration of VLP at 20 s was approximately 0.45 μM, with no significant variation detected at later times. Repeating the reaction with slightly lower reactant concentrations, in the flow-through setup, showed that, even at the lower concentration and longer reaction times (up to 4 min), there was no significant increase in the concentration of the product (Supporting Information Figure S6). This finding suggests that 0.45 μM is close to the steady-state concentration of VLPs, under the conditions of our measurements.

Master Equation Modeling of Assembly Using TR-SAXS Data. SAXS data informed development of a model of VLP assembly. Initially, two alternatives were considered. In the first model, VLPs would form by binding of $VP1_5$ to 500mer RNA (eq 4); intermediates would be partial capsids, expected to be present at low concentrations.[16] In the second alternative, 12 $VP1_5$ would form an amorphous complex with a 500mer that would then anneal to a compact VLP (eq 5).[31,32] These are the simplified models:

$$12\mathrm{VP1_5} + \mathrm{RNA} \rightarrow \mathrm{VLP} \quad (4)$$

$$12\mathrm{VP1_5} + \mathrm{RNA} \rightarrow \text{amorphous complex} \rightarrow \mathrm{VLP} \quad (5)$$

The SAXS data indicate that assembly is very rapid with no measurable intermediate concentrations, effectively a two state reaction. The annealing step is thus either very fast or altogether absent. Therefore, subsequent rigorous assembly models were based on the assumption of stepwise association of pentamers to the RNA. On the basis of previous experience with such models,[16,33] we incorporated the possibility of a rate-limiting nucleation step, where the first n subunits associated with one another and with the RNA at a slower rate and/or weaker association energy.

$$n\mathrm{VP1_5} + \mathrm{RNA} \underset{k_{\mathrm{D,nuc},j}}{\overset{k_{\mathrm{nuc},j}}{\rightleftharpoons}} \mathrm{nucleus}_n \text{ (nucleation)} \quad (6)$$

The nucleation step is followed by a series of $(12 - n)$ elongation steps:

$$\mathrm{VP1_5} + \mathrm{nucleus}_n \underset{k_{\mathrm{D},j}}{\overset{k_{\mathrm{f},j}}{\rightleftharpoons}} \mathrm{VP1_5} + \mathrm{nucleus}_{n+1} \underset{k_{\mathrm{D},j}}{\overset{k_{\mathrm{f},j}}{\rightleftharpoons}} \cdots \underset{k_{\mathrm{D},12}}{\overset{k_{\mathrm{f},12}}{\rightleftharpoons}} \mathrm{VLP} \text{ (elongation)} \quad (7)$$

Nucleation begins with the first subunit binding to RNA with a rate of $k_{\mathrm{nuc},j}$ and a dissociation rate of $k_{\mathrm{D,nuc},j}$. The index j indicates that the rate constant for association or dissociation of each pentamer will include terms for the degeneracy of assembly and disassembly and for the number of pentamer−pentamer interactions that form or break during assembly or disassembly (see ref 34). After the nucleating pentamer(s) bind, the subsequent $(12 - n)$ "elongation" reactions occur at association rates of $k_{\mathrm{f},j}$ and dissociation rates of $k_{\mathrm{D},j}$. The stability of the interactions appears in the dissociation term. For example, the last pentamer associates to a single site with a rate constant of $k_{\mathrm{f},12}$ whereas the corresponding dissociation could

dx.doi.org/10.1021/ja2110703 | J. Am. Chem. Soc. 2012, 134, 8823−8830

Table 1. Kinetic Constants[a]

constant	size of pentamer nucleus: monomeric	dimeric	trimeric	consensus
k_{nuc} (M^{-1} s^{-1})	9.3×10^7	2.2×10^7	0.9×10^7	4×10^7
ΔG_{nuc} (kcal/mol)	−6.48	−4.74	−6.03	−(5.8 ± 0.9)
k_f (M^{-1} s^{-1})	1.81×10^{10}	7.32×10^8	4.3×10^8	6×10^9
ΔG_{elong} (kcal/mol)	−2.58	−2.96	−2.54	−(2.7 ± 0.2)
k_f/k_{nuc}	201	33	48	90

[a]Constants from kinetics curve fits to the concentration of the formed $T = 1$ virus-like particles as a function of time. Simulations are based on reaction of 7.5 μM $VP1_5$ with 0.5 μM 500mer RNA. The consensus is a simple average.

occur at any of 12 equivalent sites and will require simultaneous breaking of five interpentamer contacts (and $VP1_5$-RNA contact), each with an association energy of $\Delta G^0_{contact}$. (As the dissociation constant for reaction j, $K_{D,j}$, is equal to $k_{D,j}/k_{f,j}$, the resulting dissociation rate, $k_{D,12}$ is thus $12k_{f,12}$ $\exp(-\Delta G^0_{contact}/RT)$, where R is the universal gas constant and T is temperature in Kelvin.)

Models were tested for reactions with monomeric, dimeric, and trimeric nuclei. All three models fit the data extremely well (Figure 3B and Supporting Information Figure S6). Further experiments with other initial concentrations might differentiate between different nuclei sizes.[21,35,36] Those experiments, however, are challenging because by increasing concentrations the kinetics becomes too rapid to follow by our TR-SAXS, whereas by lowering concentrations the signals become too weak to properly analyze. Residuals from comparison of observed assembly and calculated kinetic trajectories appear to be small and random and are similar for the three models (Supporting Information Figure S6). The root-mean-square deviation (rmsd) between observed and predicted values was about 7×10^{-9} M, which is ca. 1.5% of the final VLP concentration. All three models generate undetectable concentrations of intermediates, consistent with the two-state behavior suggested by the isosbestic point and fitting of the TR-SAXS curves to two basis spectra, corresponding to the product and the two reactants, using eq 3 (Figure 3A and Supporting Information Figure S4). The last panel of Supporting Information Figure S6 shows that simulations predict that less than 4% of the total VP1 concentration will ever be present as intermediate and only at early times in the reaction.

Kinetic models were fit to our TR-SAXS data to allow extraction of rate and association constants (Table 1). To simplify comparisons, microscopic rate constants and association energies are provided in Table 1. (The microscopic constants are the underlying values stripped of statistical factors for reaction degeneracy, i.e., the 5-fold symmetry of incoming pentamers and the number of available sites on a given intermediate.) Including the reaction degeneracy ($-RT$ $\ln(5^{11}/12)$),[16] the overall association energy of the capsid is thus about −95 kcal/mol ($159k_BT$). The nucleation phase of assembly is characterized by a slow rate and strong association energy compared with the elongation phase. This process is contrary to classical polymerization reactions where nucleation is characterized by weak association energy compared with that of elongation. In our case, however, nucleation is dominated by the relatively slow and relatively strong pentamer−RNA interaction. Therefore, the delineation between the nucleation and elongation phases of assembly is kinetic. Simulations indicate that elongation may be as much as 150-fold faster than nucleation. Though elongation is very fast, with an average value of 6×10^9 M^{-1} s^{-1}, the per-contact association energy for elongation is very weak: only about −2.7 kcal/mol per contact, corresponding to a 10 mM dissociation constant. Nevertheless, as each $VP1_5$ is pentavalent, the pseudocritical concentration of assembly is proportional to $^5/_2\Delta G^0_{contact}$, corresponding to 10 μM; the added energy of nucleation brings the pseudocritical $VP1_5$ concentration to between 0.6 and 2.1 μM, which compares well with the observed concentration of free pentamers of approximately 2 μM (Figure 1 and Supporting Information Figure S1).

DISCUSSION

Using 500mer RNA, we have shown that we can drive formation of $T = 1$ VLPs from SV40 $VP1_5$. Using TR-SAXS, we show that the kinetics of RNA-driven SV40 VLP formation is very fast, yet it can be described in terms of simple nucleated assembly followed by elongation steps (Figure 4). Similar models accurately describe assembly of empty capsids from many different viruses.[37] Application to experimental observation of nucleic acid-driven assembly has provided surprising results. A close examination of assembly parameters shows that the interactions of protein and nucleic acid is important for the regulation of assembly, and long-range electrostatics are imperative for attracting reactants.

Surprisingly, the binding of the first pentamers to the 500mer RNA molecule and protein−protein self-association on the RNA were astoundingly weak, about −6 kcal/mol (Table 1). Elongation energies, which are the pairwise interaction energies including contribution from nucleic acid, were even weaker, about −2.7 kcal/mol for all elongation steps (Table 1). In the assembly models, the association energy has contributions from protein−protein and protein−RNA interactions. Thus, in the monomeric nucleation model, where assembly is nucleated by the association of the first pentamer to the 500mer, the nucleation center association energy only reflects binding of $VP1_5$ to RNA (other forms of nucleation include contributions from protein−protein interaction modulated by association rate). The estimated RNA−$VP1_5$ association energy of −6.48 kcal/mol (Table 1) corresponds to a dissociation constant of 15 μM. By comparison, the dissociation constant determined for binding of $VP1_5$, truncated for its C-terminal arms, to DNA was 2−7 nM,[10] more than 3 orders of magnitude lower. These results indicate a thermodynamic barrier to binding of wt $VP1_5$ (with full C-termini) to RNA. Because the high affinity nucleic acid binding occurs in a C-terminus truncated protein,[10,38] the VP1's C-terminal arm is likely to act as governor for nucleic acid binding and assembly. This is supported by a study on chaperone-assisted assembly,[38] which appears to require a C-terminus bound protein. Indeed, the crystal structure of polyomavirus unassembled pentamers (truncated for the C-arm and part of the N-arm) shows that the conformation of the DNA binding domain (which is at the N-terminus) is altered during

dx.doi.org/10.1021/ja2110703 | J. Am. Chem. Soc. 2012, 134, 8823−8830

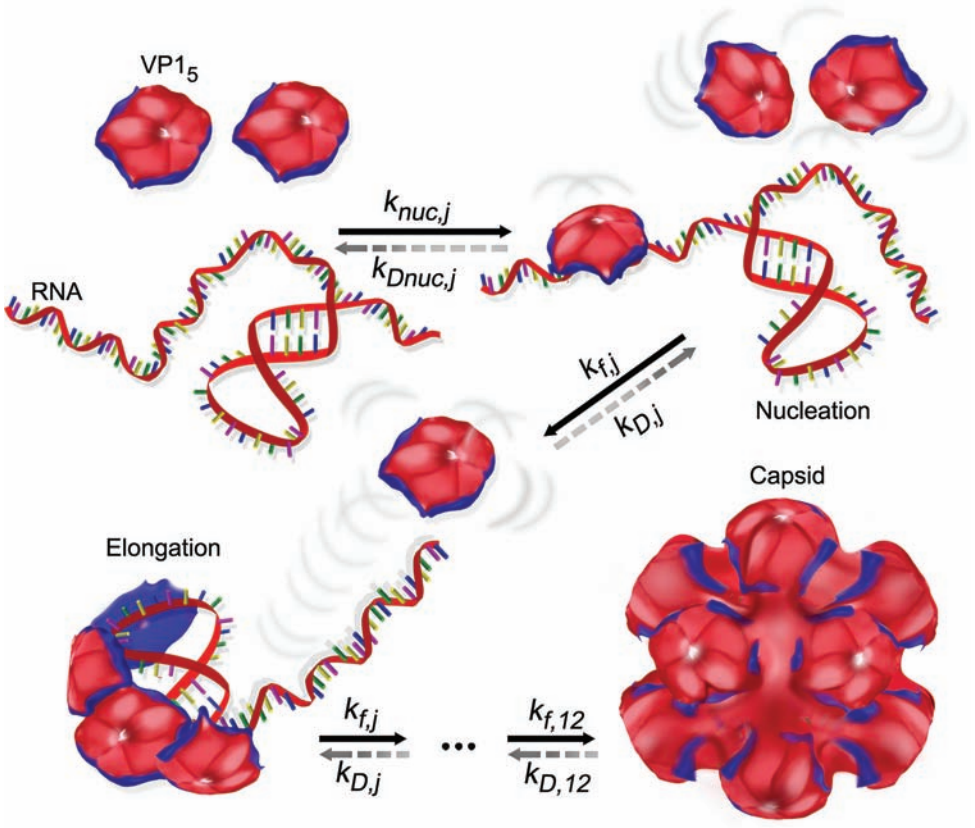

Figure 4. Nucleoprotein antenna model of assembly. The cartoon depicts assembly of SV40 VP1 pentamers on an RNA substrate. The RNA and the external surface of the pentamers are negatively charged, as indicated by the red color. The inner surface of the pentamer has a positively charged nucleic acid-binding surface, shown in blue. Thus, each pentamer is intrinsically dipolar. Free pentamers are attracted to the negatively charged RNA via their positively charged inner surface. Nucleation is shown here as attachment of a single pentamer to the RNA. The partly packaged RNA and the exterior of the growing capsid are both negatively charged and can thus function together as an antenna to attract additional capsomers. Elongation is facilitated by electrostatic attraction of pentamers and their diffusion (or sliding), along RNA and the exterior of the incomplete capsid, to the next assembly site until assembly is completed. Thus, the assembly rate continues to be very rapid throughout the assembly reaction although the RNA is progressively packaged.

assembly, suggesting that in the unassembled pentamers the C-terminus occludes the nucleic acid binding domain.[39]

The mutual occlusion of both C and N-termini was proposed as a mechanism that prevents self-invasion of C-arms into their parent-pentamer, a process that would poison assembly.[39] We propose that the conformational change, releasing both termini, is triggered by pentamer binding to the nucleic acid. This binding is followed by pentamer sliding along the nucleic acid to an appropriate position, allowing the released C-termini to connect with neighboring pentamers (Figure 4). Analysis of virus assembly thermodynamics is in its infancy: To our knowledge, only HBV and phage MS2 have previously been shown to regulate their assembly using a conformational assembly inactive state.[40−42]

It is also worth iterating that we did not observe intermediates during SV40 VLP assembly. One expectation was that we would see rapid formation of an unstructured nucleoprotein complex that would anneal.[31,32] Such would be the case if binding to nucleic acid was fast but formation of protein−protein contacts relatively slow; we observed no evidence of an initial complex that matured into the T = 1 conformation. Disordered intermediate complexes of RNA and pentamers consist of various conformations, shapes, and sizes. Each structure has a different scattering contribution to the signal. The sum of the contributions typically results in a decaying curve rather than the observed oscillating signal (Figure 3A) that well fits a well-defined structural model (Supporting Information Figure S4). The observed spectra are well-described as a linear combination of reactants (RNA and VP1$_5$) and T = 1 VLP normalized basis spectra. Furthermore, the absence of unstructured capsids indicates that there was no special barrier to self-association of subunits. Indeed, assembly was highly cooperative (Figures 1 and 3 and Supporting Information Figure S1), which indicates that protein interactions were attractive and facile.[43] Another expectation was that incorporation of the last few subunits would be very difficult. This expectation arose from simulations of assembly of empty capsids, where the last few subunits were kinetically impeded, probably by the decreasing target size,[44,45] or kinetically and thermodynamically impeded by partial blockage of the site due to capsid breathing.[46] Even if complete and nearly complete VLPs would be undistinguishable, accumulation of incomplete intermediates would contribute differently to the scattering signal than any linear combination of the basis spectra used in eq 3. Dissection, however, of the SAXS spectra in terms of RNA, VP1$_5$, and VLP was well-described by a single parameter fit (Supporting Information Figure S4 and eq 3), indicating that almost complete capsids, like other intermediates (or incomplete capsids), were not present at detectable concentrations.

dx.doi.org/10.1021/ja2110703 | J. Am. Chem. Soc. 2012, 134, 8823−8830

The kinetics of RNA-induced $VP1_5$ assembly were very fast, although 13 components (12 pentamers and an RNA molecule) participate in the reaction. In spite of the possibilities for intermediates and off-path complexes, only reactants and completed VLP were evident during the reaction. The two-state appearance is precisely the expectation for nucleated capsid assembly, where rare nuclei are rapidly consumed as soon as they appear.[16] The surprising point is that addition of the first nucleating pentamer/s to RNA was 2 orders of magnitude slower compared with subsequent elongation (Table 1). If we postulate that a conformational change is required to form the $VP1_5$–RNA interactions, the elongation reactions must be accelerated by direct interaction with the growing capsid, presumably by an induced fit mechanism.

The kinetic rate constants, for both nucleation and elongation, were stunningly fast. The elongation rates calculated from different models are lower-bound estimates of the actual association rates; the k_f values are microscopic rates that ignore degeneracy coefficients of up to 30-fold for the rate limiting steps. Unusually fast kinetics for protein–nucleic acid interactions, however, are not uncommon, facilitated by one-dimensional diffusion of positively charged protein along negatively charged nucleic acid and by long-ranged electrostatic steering.[47] Note that under the experimental (physiological) conditions the Debye screening length is between 1 and 2 nm.

All three kinetic models (Figure 3B and Supporting Information Figure S6) have two common features: the nucleation step is much slower than subsequent elongation and, surprisingly, nucleation is much lower energy than elongation (Table 1). Thus, the limiting factor of VLP assembly is the kinetics of nucleation. Editing the data causes modest changes in the quantitation of energy and rate. A simpler model based on two rate constants and a single association energy did not fit the data; this suggests that the model with unique rate and association constants for nucleation and elongation steps represents the minimal chemically realistic model. Furthermore, the summed ΔG values from the curve fit (Figure 3), as modified by entropic statistical terms, are in agreement with the overall association energy. To derive more precise reaction constants will require a global comparison of a broad range of solution conditions to master equations with differing nucleation steps (as shown in this paper) and varying selections of possible intermediates.[33,48]

Calculations and coarse-grained dynamic simulation[45,49] examined the role of nucleic acid length, and the ratio between the protein–nucleic acid and protein–protein interactions on the assembled structure and assembly mechanism. Those studies show that when the nucleic acid is short (e.g., 500mer, as in our study), smaller particles are expected.[45] A nucleation and elongation assembly mechanism is expected for short RNA when the protein–protein attraction energy is of the same order of magnitude as the protein–RNA attraction, consistent with our finding (Table 1).[45] Simulations[49] show that the capsid protein sticks to the RNA through electrostatic interactions and slides along the RNA chain toward the assembly site. This sliding process was described by von Hippel and co-workers[47] as one-dimensional diffusion and increases the rate of association. The ssRNA can similarly serve as an antenna, collecting the capsid proteins from the solution and guiding them to the assembly site (Figure 4).[49]

Coarse grained simulations support the antenna hypothesis but particularly emphasize the role of the antenna in nucleating assembly.[45,50] These calculations predict that the RNA antenna effect will be attenuated as the nucleic acid is adsorbed by the addition of pentamers. The calculations, however, dramatically understate the situation observed in the TR-SAXS experiments. We observe that assembly is very fast even when the RNA is all but encapsidated. We offer a simple explanation that is general to many viruses: the exterior of the capsid is negatively charged, while the protein's nucleic acid binding surface is positively charged, creating a huge dipole for the incoming subunit (Figure 4 and Supporting Information Figure S7). Thus, both exposed nucleic acid and the negatively charged incipient exterior of the growing capsid act together as an electrostatic attractant.[27] Though only a small gap may remain on the growing capsid, two-dimensional diffusion of the incoming subunit over the exterior surface is likely to be very fast. Postulating that the negatively charged capsid exterior, which grows during assembly, acts as an antenna leads to the distinct possibility that it will support progressively increased apparent rates of subunit addition.

■ CONCLUSIONS

We have shown that a short RNA molecule induces rapid assembly of 12 SV40 VP1 pentamers to form a $T = 1$ VLP. Our high-resolution synchrotron time-resolved solution small-angle X-ray scattering (TR-SAXS) data are consistent with a two state reaction: reactants (VP1 pentamers and RNA) and RNA-filled VLPs. Intermediate concentrations were immeasurably low. Assembly trajectories were well fit by models based on nucleated, stepwise assembly. Reaction parameters based on the models indicate that the nucleation phase was kinetically limited[21] and that interpentamer association energies were very weak. In nature the interpentamer bonding of SV40 is stabilize by Ca^{2+} ions, 2 ions per monomer (10 per pentamer), that lock the C-arms in neighboring pentamers.[11] The kinetics of the reaction has interesting implications for assembly *in vivo*. Hypothetically, once assembly is initiated, speed and cooperativity will allow viruses to assemble with minimal interference from host defenses. The basis of the speed of assembly is likely to be the long-range electrostatic interactions afforded by the positive charge of the incoming subunit ($VP1_5$), attracted to the negative charge of the nucleic acid and the negative charge of the exterior of the growing capsid. As evidence of external negative charge, many viruses, including SV40, migrate to the anode during native agarose gel electrophoresis (Figure 1 and Supporting Information Figure S1). One can speculate that viruses use this charge to achieve the antenna effect in the crowded environs of the cell.

■ ASSOCIATED CONTENT

Supporting Information

Additional supporting figures (Figures S1–S7) and data analysis. This material is available free of charge via the Internet at http://pubs.acs.org.

■ AUTHOR INFORMATION

Corresponding Author

raviv@chem.ch.huji.ac.il; azlotnic@indiana.edu; ariella.oppenheim@mail.huji.ac.il

Author Contributions

$^{\nabla}$These authors contributed equally.

Notes

The authors declare no competing financial interest.

■ ACKNOWLEDGMENTS

We gratefully acknowledge use of the ID02 beamline at the ESRF synchrotron and thank J. Gummel, S. Callow, and T. Naryanan for experimental help and useful discussions. We thank the SWING beamline and J. Perez and his team at the SOLEIL synchrotron for experimental support and W. M. Gelbart for helpful discussions. Micrographs were recorded at the Indiana Molecular Biology Institute EM facility. Support for this project was provided by the Safra, Wolfson, and Rudin foundations (U.R.), the James Franck and Fritz Haber Minerva Centers (U.R. and D.H.), the Hebrew University Nanocenter (R.A.), the US−Israel Binational Science Foundation (BSF) (Grant Number 2005050; A.O. and A.Z.), and NIH R01-AI077688 (A.Z.).

■ REFERENCES

(1) Young, M.; Willits, D.; Uchida, M.; Douglas, T. *Annu. Rev. Phytopathol.* **2008**, *46*, 361.
(2) Kang, S.; Uchida, M.; O'Neil, A.; Li, R.; Prevelige, P. E.; Douglas, T. *Biomacromolecules* **2010**, *11*, 2804.
(3) Aniagyei, S. E.; Dufort, C.; Kao, C. C.; Dragnea, B. *J. Mater. Chem.* **2008**, *18*, 3763.
(4) Dragnea, B. *Nat. Mater.* **2008**, *7*, 102.
(5) Kimchi-Sarfaty, C.; Ben-Nun-Shaul, O.; Rund, D.; Oppenheim, A.; Gottesman, M. M. *Hum. Gene Ther.* **2002**, *13*, 299.
(6) Arad, U.; Zeira, E.; El-Latif, M. A.; Mukherjee, S.; Mitchell, L.; Pappo, O.; Galun, E.; Oppenheim, A. *Hum. Gene Ther.* **2005**, *16*, 361.
(7) Li, W.; Asokan, A.; Wu, Z.; Van Dyke, T.; DiPrimio, N.; Johnson, J. S.; Govindaswamy, L.; Agbandje-McKenna, M.; Leichtle, S.; Redmond, D. E. Jr.; McCown, T. J.; Petermann, K. B.; Sharpless, N. E.; Samulski, R. J. *Mol. Ther.* **2008**, *16*, 1252.
(8) Griffith, J.; Dieckmann, M.; Berg, P. *J. Virol.* **1975**, *15*, 167.
(9) Varshavsky, A. J.; Bakayev, V. V.; Chumackov, P. M.; Georgiev, G. P. *Nucleic Acids Res.* **1976**, *3*, 2101.
(10) Li, P. P.; Nakanishi, A.; Shum, D.; Sun, P. C.; Salazar, A. M.; Fernandez, C. F.; Chan, S. W.; Kasamatsu, H. *J. Virol.* **2001**, *75*, 7321.
(11) Stehle, T.; Gamblin, S. J.; Yan, Y.; Harrison, S. C. *Structure* **1996**, *4*, 165.
(12) Li, P. P.; Nakanishi, A.; Clark, S. W.; Kasamatsu, H. *Proc. Natl. Acad. Sci. U.S.A.* **2002**, *99*, 1353.
(13) Liddington, R. C.; Yan, Y.; Moulai, J.; Sahli, R.; Benjamin, T. L.; Harrison, S. C. *Nature* **1991**, *354*, 278.
(14) Sandalon, Z.; Oppenheim, A. *Virology* **1997**, *237*, 414.
(15) Mukherjee, S.; Abd-El-Latif, M.; Bronstein, M.; Ben-nun-Shaul, O.; Kler, S.; Oppenheim, A. *PLoS One* **2007**, *2*, e765.
(16) Katen, S. P.; Zlotnick, A. *Methods Enzymol.* **2009**, *455*, 395.
(17) Rapaport, D. C. *Phys. Rev. Lett.* **2008**, *101*, 186101.
(18) Zlotnick, A. *J. Mol. Biol.* **2007**, *366*, 14.
(19) Prevelige, P. E.; Thomas, D.; King, J. *Biophys. J.* **1993**, *64*, 824.
(20) Zlotnick, A.; Aldrich, R.; Johnson, J. M.; Ceres, P.; Young, M. J. *Virology* **2000**, *277*, 450.
(21) Zlotnick, A.; Johnson, J. M.; Wingfield, P. W.; Stahl, S. J.; Endres, D. *Biochemistry* **1999**, *38*, 14644.
(22) Porterfield, J. Z.; Dhason, M. S.; Loeb, D. D.; Nassal, M.; Stray, S. J.; Zlotnick, A. *J. Virol.* **2010**, *84*, 7174.
(23) Johnson, J. M.; Tang, J.; Nyame, Y.; Willits, D.; Young, M. J.; Zlotnick, A. *Nano Lett.* **2005**, *5*, 765.
(24) Johnson, J. M.; Willits, D.; Young, M. J.; Zlotnick, A. *J. Mol. Biol.* **2004**, *335*, 455.
(25) Mukherjee, S.; Kler, S.; Oppenheim, A.; Zlotnick, A. *Virology* **2010**, *397*, 199.
(26) Szekely, P.; Ginsburg, A.; Ben-Nun, T.; Raviv, U. *Langmuir* **2010**, *26*, 13110.
(27) Szekely, O.; Steiner, A.; Szekely, P.; Amit, E.; Asor, R.; Tamburu, C.; Raviv, U. *Langmuir* **2011**, *27*, 7419.
(28) Nadler, M.; Steiner, A.; Dvir, T.; Szekely, O.; Szekely, P.; Ginsburg, A.; Asor, R.; Resh, R.; Tamburu, C.; Peres, M.; Raviv, U. *Soft Matter* **2011**, *7*, 1512.
(29) Hammersley, A. P.; Svensson, S. O.; Hanfland, M.; Fitch, A. N.; Hausermann, D. *High Pressure Res.* **1996**, *14*, 235.
(30) Ben-Nun, T.; Ginsburg, A.; Szekely, P.; Raviv, U. *J. Appl. Crystallogr.* **2010**, *43*, 1522.
(31) McPherson, A. *Bioessays* **2005**, *27*, 447.
(32) Hagan, M. F. *J. Chem. Phys.* **2009**, *130*, 114902.
(33) Moisant, P.; Neeman, H.; Zlotnick, A. *Biophys. J.* **2010**, *99*, 1350.
(34) Zlotnick, A. *J. Mol. Biol.* **1994**, *241*, 59.
(35) Endres, D.; Zlotnick, A. *Biophys. J.* **2002**, *83*, 1217.
(36) Hagan, M. F.; Elrad, O. M. *Biophys. J.* **2010**, *98*, 1065.
(37) Zlotnick, A.; Mukhopadhyay, S. *Trends Microbiol.* **2011**, *19*, 14.
(38) Chromy, L. R.; Pipas, J. M.; Garcea, R. L. *Proc. Natl. Acad. Sci. U. S. A.* **2003**, *100*, 10477.
(39) Stehle, T.; Harrison, S. C. *EMBO J.* **1997**, *16*, 5139.
(40) Ceres, P.; Zlotnick, A. *Biochemistry* **2002**, *41*, 11525.
(41) Packianathan, C.; Katen, S. P.; Dann, C. E. 3rd; Zlotnick, A. *J. Virol.* **2010**, *84*, 1607.
(42) Stockley, P. G.; Rolfsson, O.; Thompson, G. S.; Basnak, G.; Francese, S.; Stonehouse, N. J.; Homans, S. W.; Ashcroft, A. E. *J. Mol. Biol.* **2007**, *369*, 541.
(43) McGhee, J. D.; von Hippel, P. H. *J. Mol. Biol.* **1974**, *86*, 469.
(44) Rapaport, D. C. *Phys. Rev. E: Stat. Nonlin. Soft Matter Phys.* **2004**, *70*, 051905.
(45) Elrad, O. M.; Hagan, M. F. *Phys. Biol.* **2010**, *7*, 045003.
(46) Nguyen, H. D.; Reddy, V. S.; Brooks, C. L. 3rd. *Nano Lett.* **2007**, *7*, 338.
(47) von Hippel, P. H.; Berg, O. G. *J. Biol. Chem.* **1989**, *264*, 675.
(48) Endres, D.; Miyahara, M.; Moisant, P.; Zlotnick, A. *Protein Sci.* **2005**, *14*, 1518.
(49) Hu, T.; Shklovskii, B. I. *Phys. Rev. E: Stat. Nonlin. Soft Matter Phys.* **2007**, *75*, 051901.
(50) Kivenson, A.; Hagan, M. F. *Biophys. J.* **2010**, *99*, 619.